Pyrene Eximer Mapping in Cultured Fibroblasts by Ratio Imaging and Time-Resolved Microscopy†

James A. Dix and A. S. Verkman*

Departments of Medicine and Physiology, Cardiovascular Research Institute, University of California, San Francisco, California 94143-0532

Received July 13, 1989; Revised Manuscript Received October 18, 1989

ABSTRACT: The kinetics of pyrene eximer formation provide a measure of lateral diffusibility in bilayer membranes. Swiss 3T3 fibroblasts were labeled with pyrene, pyrenedecanoic acid (PDA) and 1,3-bis(1-pyrene)propane (BPP) by incubation in the presence of Pluronic F127. Single-cell emission spectra obtained by epifluorescence microscopy (excitation 350 nm) with photodiode array detection showed monomer (380–420 nm) and eximer (475 nm) peaks. The eximer-to-monomer fluorescence ratio (E/M) increased with increasing temperature and loading time. Time-resolved microscopy studies of fibroblasts labeled with PDA for 15 min gave monomer and eximer lifetimes of 101 and 78 ns, respectively, with a monomer-to-eximer conversion rate of 0.02 ns^{-1}. E/M ratio images were obtained with a microchannel plate intensifier and CCD camera at 350-nm excitation and 405 ± 5 nm (monomer) and >470-nm (eximer) emission wavelengths. E/M ratios of PDA showed spatial variation across the cell with highest ratios at the peripheral plasma membrane. These results establish the methodology to label cells with pyrene eximer-forming probes and to image eximer distributions in membranes of intact cultured cells. Eximer-to-monomer fluorescence ratios are sensitive to maneuvers that alter the membrane physical state and should be of utility in examining the cellular regulation of membrane fluidity.

The dynamic physical properties of cell membranes have an important role in the complex modulation of membrane barrier and protein function. Much of our understanding of membrane fluidity or "microviscosity" is based on studies of the rotational dynamics of fluidity-sensitive fluorophores in isolated phospholipid and biological membrane vesicles. Although these studies give important information about the membrane phase state and the influence of lipid composition on fluidity, they do not give information about the dynamic interactions between membrane fluidity and cellular metabolism in intact cells. Recently, we introduced methodology to image with spatial resolution the anisotropy of fluidity-sensitive fluorophores such as trimethylammonium diphenylhexatriene (TMA-DPH) (Dix & Verkman, 1990; Fushimi et al., 1990). This approach gave real-time information about the rotational mobility of fluorescent probes in intracellular and plasma membranes.

It has been recognized that the rotational mobility of fluorescent or magnetic resonance probes in membranes is in general quite different from the lateral diffusibility (Edidin, 1974; Hughes et al., 1982). Long-range lateral diffusion has been studied by the fluorescence photobleaching recovery technique in which the translational diffusion of fluorophores into a photobleached area of membrane is measured (Axelrod et al., 1976). Short-range lateral diffusion has been assessed indirectly from the rate of eximer formation of lipophilic fluorophores such as pyrenes that undergo intra- or intermolecular eximer formation (Galla & Hartmann, 1980; Melnick et al., 1981). Mathematical models have been developed to relate the kinetics of eximer formation to lateral diffusion coefficients (Eisinger et al., 1986).

The ratio of steady-state eximer-to-monomer fluorescence emission provides a simple measure of the kinetics of eximer formation. We report here the application of ratio imaging to map the kinetics of eximer formation in intact cultured cells. Because eximer mapping in intact cells has not been reported previously, it was necessary to (a) establish cell labeling procedures to obtain adequate monomer and eximer fluorescence signals, (b) validate that eximer formation occurred, and (c) apply quantitative ratio imaging to measure eximer-to-monomer fluorescence ratios with spatial resolution. Methodology was developed to label monolayer cultured cells with pyrene derivatives and to obtain eximer images. Results were validated by use of single-cell spectroscopy and nanosecond time-resolved microscopy. Applications and limitations of this eximer imaging technique are discussed.

Materials and Methods

Chemicals. Pluronic F127, 1-pyrenedecanoic acid (PDA) and 1,3-bis(1-pyrene)propane (BPP) were obtained from Molecular Probes (Eugene, OR). All other chemicals were obtained from Sigma Chemical Co. (St. Louis, MO).

Cell Culture and Fluorescence Labeling. Swiss 3T3 fibroblasts (ATCC CCL 92) were obtained from the Cell Culture Facility at UCSF and used between passages 121 and 128. Cells were grown at 37 °C in 5% CO_2–95% air in Dulbecco's modified Eagle's medium supplemented with 10% fetal bovine serum, penicillin (100 units/mL), and streptomycin (100 μg/mL). Cells were grown to confluence on thin glass cover slips (18-mm diameter).

Monolayer confluent cells were rinsed with 20 mL of 101 mM NaCl, 5 mM KCl, 2 mM $MgCl_2$, 2 mM $CaCl_2$, 5 mM D-glucose, 50 mM mannitol, and 5 mM Hepes/Tris, pH 7.4 (buffer A), and mounted in a cell perfusion chamber for continuous perfusion at constant temperature (Chao et al.,

†This work was supported by Grants DK35124, DK39354, and HL42368 from the National Institutes of Health, a grant-in-aid from the American Heart Association, and grants from the National Cystic Fibrosis Foundation and the Johns Hopkins Center for Alternatives to Animal Testing. A.S.V. is an Established Investigator of the American Heart Association.

* Address correspondence to this author.

0006-2960/90/0429-1949$02.50/0

1989). Cells were incubated at 23 °C in the dark in buffer A containing 0.08% Pluronic F127 and the pyrene probe for specified times. Pluronic F127 is used frequently at this or higher concentrations without toxicity to load calcium indicators into cells.

Image Analysis. Fluorescently labeled cells were viewed with an inverted epifluorescence microscope (Nikon Diaphot-TMD-EF, Nippon Kogaku, Tokyo, Japan). All glass optics in the excitation path were replaced with fused silica. Fluorescence was excited by a 100-W Hg arc lamp in series with an OD 2 neutral density filter. Excitation light was filtered by a 350-nm six-cavity dichroic interference filter (bandwidth 10 nm; Omega Optical Co., Brattleboro, VT) and reflected into the perfusion chamber by a fused silica 20% reflective, partially silvered dichroic mirror or a 370-nm dichroic (Omega Optical). Emitted light was filtered by a six-cavity 405-nm interference filter (10-nm bandwidth) for monomer fluorescence and a 470-nm cut-on filter for eximer fluorescence. A sliding mount was constructed to change rapidly between emission filters without disturbing the optical path. Cells were viewed with a 40× Fluor objective (Nikon, 1.3 N.A., oil immersion, 0.17-mm working distance).

The image was focused onto a variable-gain, microchannel plate image intensifier (Videoscope International, Washington, DC) and imaged with a solid-state CCD camera (Cohu, San Diego, CA) operating at fixed gain. The output of the CCD camera was digitized with a frame grabber (DT2861, Data Translation, Marlboro, MA) in a 80286 computer with 80287 math coprocessor (Rose Hill, Scotts Valley, CA). An auxiliary processing board (DT2858, Data Translation) was used to speed frame processing; 512 × 512 × 8 bit images were stored on a dedicated 110 MB hard disk drive. Data acquisition and analysis software was written in Microsoft FORTRAN 4.0.

The linearity and flatness of the imaged field were confirmed as described previously (Dix & Verkman, 1990). Background images at the monomer and eximer emission wavelengths were obtained with unlabeled cells before labeling in situ in the perfusion chamber. Background was generally <5% of total signal and subtracted from images of loaded cells. Acquisition of individual images required 5 s of image averaging. There was no photobleaching when cells were illuminated only during image acquisition. Ratio images of the fluorescence at the eximer-to-monomer emission wavelengths were calculated pixel-by-pixel and displayed on a gray scale. When necessary, images were displaced in the x and y directions by an integral number of pixels (always <5) to align monomer and eximer images. Slight misregistration of images sometimes occurred when emission filters were changed.

Single-Cell Fluorescence Spectroscopy. Emission spectra were measured by epifluorescence microscopy using a cooled, blue-intensified photodiode array (1024 diodes, EG&G, Salem, MA) and Model 1461 detector interface (Princeton Applied Research, Princeton, NJ). Emitted light was focused onto a circular-to-rectangular fused silica fiberoptic cable. The output light from the rectangular end of the cable passed into the polychromator through a narrow slit to give ~5-nm resolution. The photodiode array channel vs wavelength relation was calibrated with four narrow band-pass interference filters (405–530 nm).

Spectra were obtained with the same optical arrangement as used for imaging experiments except that emitted light was filtered through a low-autofluorescence 375-nm cut-on filter. A variable-diameter iris diaphragm was used to illuminate a selected field for spectral acquisition; 10–100 exposures (each 100 ms) were averaged to obtain spectra with signal-to-noise ratios >20. Background spectra from unlabeled cells were subtracted; intensities at each emission wavelength were generally <5% of that from labeled cells.

Time-Resolved Fluorescence Microscopy. Fluorescence lifetimes were measured by interfacing a nanosecond pulsed lifetime instrument (LS-1, PTI, London, ON, Canada) to the epifluorescence microscope. Time-dependent fluorescence was measured by replacing the Hg arc lamp source and intensifier/camera by a nanosecond N_2 flashlamp and gated photomultiplier from the PTI instrument. The flashlamp was operated at 5.4 kV at a repetition rate of 25 kHz. Typically, 50 scans of 200 data points (each data point representing 25 A/D conversions) were averaged over 12 min.

The flashlamp profile at the excitation wavelength was determined by replacing the cell perfusion chamber with a front-surfaced mirror and removing the emission filter. The flashlamp profile was measured periodically during the course of an experiment and was usually constant to within one data point. Lifetime analysis was performed by using software purchased from PTI.

Results

Experiments were performed to establish procedures to label fibroblasts grown in monolayer culture with pyrene eximer-forming probes. Vigorous agitation methods that have been used to label liposomes with pyrenes could not be used for intact adherent cells because of cell trauma. Three methods were evaluated for cell labeling. Cells were incubated in buffer A to which 1–10 μM pyrene probe was added from an ethanol or DMSO stock. No labeling of PDA, pyrene, or BPP was detected at up to 2 h of incubation at 15 or 37 °C, probably because of the very low water solubility of pyrenes. To maintain the pyrene probe in suspension, liposome transfer was tested. Pyrene probes were incorporated into 0.1–0.3 μm unilamellar phosphatidylcholine vesicles by cosonication at a 4% mole fraction. Cells were incubated with liposomes at 15 or 37 °C with a pyrene probe (aqueous) concentration of 1–20 μM. Weak labeling of PDA and pyrene was detected at 1 h with signal-to-background ratios of <2 (see below).

Efficient labeling was obtained with Pluronic F127, a detergent known to facilitate the incorporation of lipophilic compounds into membranes (Poenie et al., 1986). Cells were incubated with 0.08% Pluronic F127 containing the pyrene probe added from an ethanol or DMSO stock solution. Cell labeling was followed in situ by single-cell fluorescence spectroscopy. Adequacy of cell labeling was judged from the monomer and eximer fluorescence signals compared to background signal measured prior to labeling.

Figure 1 shows the pyrene probe emission spectra measured as a function of labeling time. Background signal has been subtracted. The fine structure of the pyrene monomer emission spectra was not observed because of the 375-nm cut-on filter in the emission path and the limited resolution of the photodiode array detection system. The total cell fluorescence signal and the eximer-to-monomer emission ratio increased with time as the density of membrane-associated PDA and pyrene increased. Adequate labeling with good eximer fluorescence and signal-to-background ratios >10:1 was obtained in 15 min with PDA and in 8 min with pyrene. Eximer-to-monomer emission ratios varied by <10% in different cells. In response to removal of the pyrene probe and continuous perfusion with buffer A, the monomer and eximer fluorescence signals from PDA decreased by <10% in 30 min at 24 °C, indicating that labeling was not easily reversed. However, the labeling with pyrene was reversed with a half-time of 8–10 min at 24 °C. Incorporation of BPP was very difficult. Labeling was first

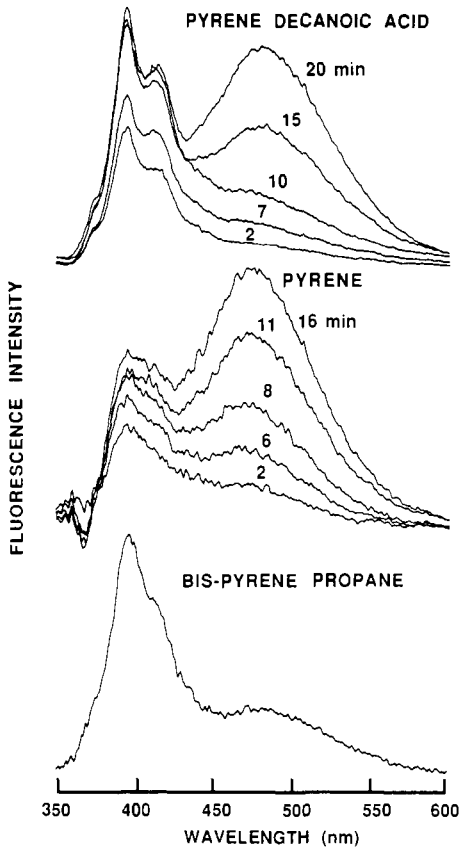

FIGURE 1: Uptake of pyrene probes by Swiss 3T3 fibroblasts at 24 °C. Cells were labeled for the specified length of time with 4 μM probe and 0.08 wt % Pluronic F127 in situ in the perfusion chamber. Single-cell spectra were then obtained after perfusion with probe-free buffer for 3 min. The BPP spectrum was obtained after 6 h of loading. The decrease in intensity below 400 nm is due to the 375-nm barrier filter in the epifluorescence filter cube.

measurable after a 2-h incubation in the presence of Pluronic F127. The total fluorescence signal increased steadily over 8 h with little change in eximer-to-monomer ratio, as predicted for intramolecular eximer formation. BPP labeling was not reversed measurably in 1 h.

Eximer-to-monomer ratios decreased markedly when fluorescence photobleaching occurred. Cell illumination with the unattenuated arc lamp at 350 nm reduced by 50% the eximer-to-monomer ratio of PDA in 1 min. Photobleaching was not detectable over 5 min when the excitation light was attenuated 400-fold. The influence of solution oxygen content was examined by perfusing cells labeled with PDA for 15 min with buffer A that was bubbled for 30 min with 100% O_2 or 100% N_2. Total fluorescence and the eximer-to-monomer ratio differed by <10%, showing little sensitivity of membrane-associated PDA to oxygen content.

To test the sensitivity of the PDA emission spectrum to a maneuver known to alter membrane fluidity, the influence of temperature was examined. Spectra were measured at different temperatures in cells loaded with PDA for 15 min (Figure 2). In one set of measurements typical of two, the eximer-to-monomer ratio increased by 23% over a 16–35 °C temperature range. Spectra were repeatable after multiple temperature changes, confirming that little loss of PDA and photobleaching occurred. This small change in eximer-to-monomer ratio is similar to the temperature dependence of pyrene eximer formation in dipalmitoyllecithin vesicles containing 30 mol % cholesterol (Galla & Sackmann, 1974).

Nanosecond lifetime studies of PDA-labeled fibroblasts were performed to confirm that spectral changes resulted from

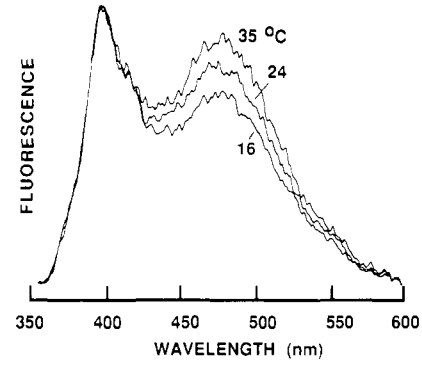

FIGURE 2: Temperature dependence of emission spectrum of pyrenedecanoic acid in Swiss 3T3 fibroblasts. Cells were labeled with 4 μM PDA and 0.08 wt % Pluronic F127 for 15 min at 24 °C. A spectrum was recorded after perfusion with buffer A at 24 °C for 3 min. Additional spectra were recorded after the cells were perfused with buffer A at 35 and 16 °C, each for 3 min. A final spectrum recorded at 24 °C was not different from the first spectrum at 24 °C (not shown). Spectra were normalized to the monomer peak fluorescence.

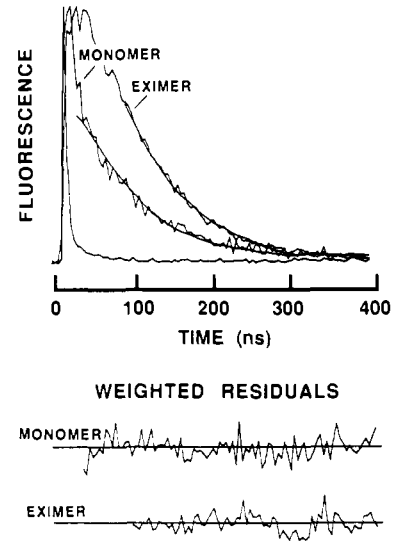

FIGURE 3: Lifetime decay of pyrenedecanoic acid in Swiss 3T3 fibroblasts. Cells were labeled with 4 μM PDA and 0.08 wt % Pluronic F127 for 15 min and then perfused continuously with buffer A. The narrow curve is the flashlamp profile. Fitted lifetimes were 51 ± 3 ns (monomer) and 78 ± 2 (eximer). Fitted lifetime of PDA in the absence of eximer was 101 ± 15 ns (not shown).

eximer formation and to evaluate eximer kinetic parameters. Figure 3 shows the nanosecond decay of PDA fluorescence. The monomer lifetime decreased from 101 ns in the absence of eximer (4-min labeling), to 51 ns in the presence of eximer (15-min labeling). These results give a monomer lifetime of 101 ns and a monomer-to-eximer conversion rate (pseudo-first-order rate constant) of 0.02 ns^{-1}. The eximer fluorescence decay showed a delay in peak fluorescence as expected for excited-state reaction kinetics and an eximer lifetime of 78 ns.

Ratio imaging was performed to resolve regions of different eximer-to-monomer ratios in a single microscope field. Figure 4 shows monomer (left) and eximer (middle) images of fibroblasts labeled with PDA for 15 min. The images show nonselective staining of cell membranes with characteristic staining of nuclear and plasma membranes. Similar staining patterns were observed with pyrene and BPP labeling (not shown). The large round nuclear membrane, along with adjacent endoplasmic reticulum, was stained brightly; nucleoli were not stained. The plasma membrane bounding the cy-

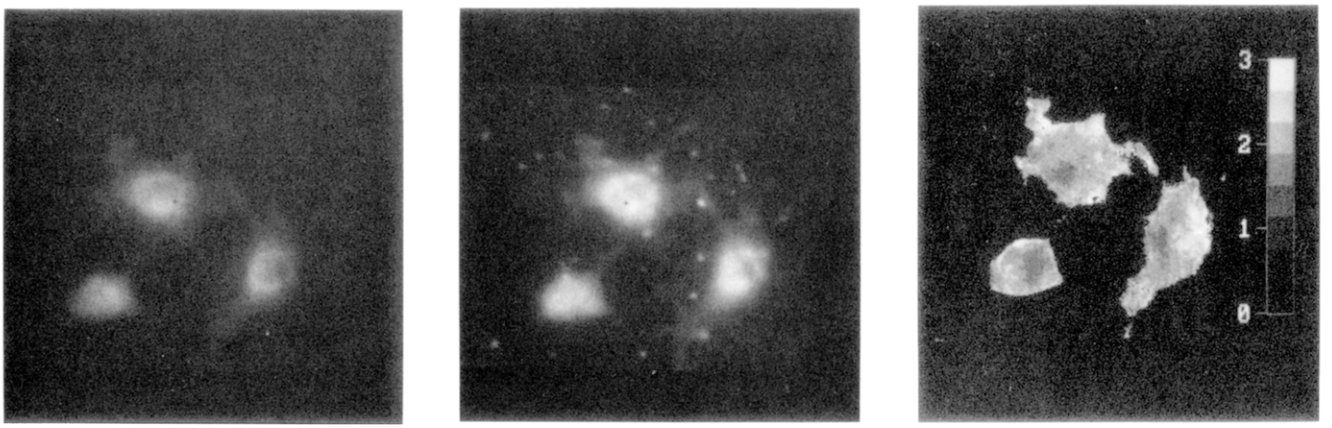

FIGURE 4: Ratio image of eximer-to-monomer fluorescence of pyrenedecanoic acid in Swiss 3T3 cells. Cells labeled with 5 μM PDA and 0.08 wt % Pluronic F127 for 15 min were imaged at 405 nm (monomer, left) and >475 nm (eximer, middle). Background images were obtained prior to labeling and were subtracted. A pixel-by-pixel ratio image (right) was then calculated as described under Materials and Methods.

toplasmic projections was stained dimly. The middle image shows bright punctate areas of fluorescence that were not seen in the monomer image. These bright dots were sometimes present when cells were not washed vigorously after labeling with PDA and represent PDA in high concentration in "droplets" of Pluronic F127. The high concentration of PDA resulted in strong eximer fluorescence and quenching of monomer fluorescence.

The gray-scale eximer-to-monomer ratio image is shown at the right in Figure 4. A threshold mask was applied to blacken regions of the ratio image where the intensity of the monomer image was <10% above background. The three cells show the lowest eximer-to-monomer ratios at the nuclear membrane and the highest ratio at the cytoplasmic membrane. This difference remained at 20 min after the 15-min labeling period, suggesting that it was not the result of labeling disequilibrium. The image also showed small dots of very high eximer-to-monomer ratio corresponding to the droplets of Pluronic F127 that adhered to cells in the eximer image. A similar ratio image was recorded for pyrene-labeled fibroblasts; however, the labeling by BPP was inadequate to produce an acceptable ratio image.

Discussion

The purpose of these studies was to develop and validate an approach to map membrane fluidity in intact cells by use of pyrene eximer formation. Eximer formation is associated with a red shift in the steady-state emission fluorescence spectrum, a decrease in monomer lifetime, and a characteristic time-resolved decay of eximer fluorescence resulting from excited-state reaction kinetics. The rate of eximer formation, assessed from steady-state or time-resolved measurements, has been taken to be a measure of the collisional rate between an excited-state and ground-state monomer and thus a measure of the translational or lateral mobility of the eximer-forming fluorescent probe (Galla & Hartmann, 1980; Eisinger et al., 1986). The information about membrane structure obtained from eximer kinetics is different from but complementary to that obtained by fluorescence anisotropy studies of probe rotation or photobleaching recovery studies of long-range translational mobility.

Three eximer-forming probes were chosen for this study because of their distinct and important properties. PDA and pyrene undergo intermolecular eximer formation. PDA and similar charged pyrene compounds have been used widely to assess diffusional mobility in phospholipid vesicles (Muller & Galla, 1987; Ollmann et al., 1988; Macdonald et al., 1988), biological membrane vesicles (Zachariasse et al., 1982; Gatt & Fibach, 1988), and blood cells in suspension (Eisinger et al., 1986; Masuda et al., 1987). In analogy to the charged DPH derivatives, it was predicted that the charged moiety would anchor the pyrene to the headgroup region of the plasma membrane to reduce probe internalization and washout. In contrast, pyrene should enter all lipidic intracellular spaces. The bis(pyrene) BPP should also label all lipid compartments; however, its ability to form intramolecular eximers has two important advantages for use in intact cells: eximer-to-monomer ratios are independent of the probe density in the membrane, and less membrane labeling is required to give adequate eximer intensities (Melnick et al., 1981; Zacharaisse et al., 1984; Storch & Schacter, 1984).

To establish cell labeling procedures, single-cell spectroscopy was performed. Adequate labeling required the use of Pluronic F127; probe incorporation by addition from an ethanol or DMSO stock solution by transfer from phospholipid vesicles was ineffective. The eximer-to-monomer fluorescence emission ratio increased over 15 min for PDA and pyrene, but over 6 h for BPP. As predicted, the rate of eximer formation was temperature dependent and, for PDA and pyrene, concentration dependent. It was necessary to excite fluorescence with a low light intensity to eliminate photobleaching which caused a drop in the eximer-to-monomer ratio. Nanosecond lifetime studies confirmed that spectral changes resulted from formation of pyrene eximers rather than from chemical modification of the pyrene monomer by intracellular metabolic processes.

PDA labeling in fibroblasts was not confined to the plasma membrane but strongly labeled nuclear and probably other intracellular membranes. A similar labeling pattern was observed for pyrene and BPP; however, the labeling and unlabeling kinetics were quite different. PDA labeled cells rapidly and washed out very slowly, while pyrene labeled rapidly and washed out rapidly; the intramolecular eximer-former BPP labeled cells very slowly. Thus, of the probes available at present, PDA has the best properties for studies in intact cells. Other similar compounds having a pyrene chromophore linked to a charged moiety, including 1-pyrenebutanoic acid and (1-pyrenylbutyl)trimethylammonium bromide, gave labeling patterns and signal-to-background ratios similar to those for PDA.

The mapping of eximer kinetics in single cells provides a potentially valuable approach to examine cell membrane fluidity and, particularly, real-time changes in fluidity in response to physical or biochemical stimuli. Eximer-to-monomer ratios are not sensitive to tissue geometry such as microvilli because a ratio imaging approach is used. However, there are

a number of concerns and cautions in the interpretation of eximer images. Determination of absolute diffusion coefficients for probes that undergo intermolecular eximer formation is not possible because of uncertainties in the probe density. In addition, eximer formation requires relatively high probe densities which might perturb membrane structure. Eximer-to-monomer ratios for probes that undergo intramolecular eximer formation are independent of probe density; however, they are likely to be sensitive to the exact position of the probe in the membrane and the details of the anisotropic membrane environment (Melnick et al., 1981). Synthesis of intramolecular eximer-forming probes that can be targeted to specific membranes in intact cells would be an important advance.

In view of these limitations, the mapping of cell eximer fluorescence is a relatively simple procedure that gives information about the membrane physical state complementary to that obtained by fluorescence photobleaching recovery and anisotropy imaging techniques. Eximer mapping should have application to real-time studies of fluidity in intracellular and plasma membranes in cultured cells and intact biological tissues.

Registry No. PDA, 60177-21-1; DPP, 61549-24-4; pyrene, 129-00-0.

References

Axelrod, D., Koppel, D. E., Schlessinger, J., Elson, E., & Webb, W. W. (1976) *Biophys. J. 16*, 1055–1069.

Chao, A. C., Dix, J. A., Sellers, M. C., & Verkman, A. S. (1989) *Biophys. J. 56*, 1071–1081.

Dix, J. A., & Verkman, A. S. (1990) *Biophys. J. 57*, 231–240.

Edidin, M. (1974) *Annu. Rev. Biophys. Bioeng. 3*, 179–201.

Eisinger, J., Flores, J., & Petersen, W. P. (1986) *Biophys. J. 49*, 987–1001.

Fushimi, K., Dix, J. A., & Verkman, A. S. (1990) *Biophys. J. 57*, 241–254.

Galla, H.-J., & Sackmann, E. (1974) *Biochim. Biophys. Acta 339*, 103–115.

Galla, H.-J., & Hartmann, W. (1980) *Chem. Phys. Lipids 27*, 199–219.

Gatt, S., & Fibach, E. (1988) *Biochim. Biophys. Acta 943*, 447–453.

Hughes, B. D., Pailthorpe, B. A., White, L. R., & Sawyer, W. H. (1982) *Biophys. J. 37*, 673–676.

Macdonald, A. G., Wahle, K. W. J., Cossins, A. R., & Behan, M. K. (1988) *Biochim. Biophys. Acta 938*, 231–242.

Masuda, M., Kuriki, H., Komiyama, Y., Nishikado, H., Egawa, H., & Murata, K. (1987) *J. Immunol. Methods 96*, 225–237.

Melnick, R. L., Haspel, H. C., Goldenberg, M., & Greenbaum, L. M. (1981) *Biophys. J. 34*, 499–515.

Muller, H.-J., & Galla, H.-J. (1987) *Eur. Biophys. J. 14*, 485–491.

Ollmann, M., Robitzki, A., Schwarzmann, G., & Galla, H.-J. (1988) *Eur. Biophys. J. 16*, 109–112.

Poenie, M., Alderton, J., Steinhardt, R., & Tsien, R. (1986) *Science 233*, 886–888.

Storch, J., & Schachter, D. (1984) *Biochemistry 23*, 1165–1170.

Zachariasse, K. A., Vaz, W. L. C., Sotomayor, C., & Kuhnle, W. (1982) *Biochim. Biophys. Acta 688*, 323–332.

Zachariasse, K. A., Duveneck, G., & Busse, R. (1984) *J. Am. Chem. Soc. 106*, 1045–1051.

Ovothiols as Free-Radical Scavengers and the Mechanism of Ovothiol-Promoted NAD(P)H–O_2 Oxidoreductase Activity†

Tod P. Holler and Paul B. Hopkins*

Department of Chemistry, University of Washington, Seattle, Washington 98195

Received June 8, 1989; Revised Manuscript Received October 9, 1989

ABSTRACT: Racemic ovothiol A [(±)-**1a**] and the ovothiol model compound 1,5-dimethyl-4-mercaptoimidazole (DMI, **2**) were found to scavange the free radicals Fremy's salt (**4**) and Banfield's radical (**5**) much more rapidly than did the thiol antioxidant glutathione. Ovothiol A also scavenges the tyrosyl radical, with efficiency comparable to that of ascorbic acid and the tocopherol analogue trolox (**3**). The ovothiol model compound DMI was found to scavenge superoxide with a rate constant comparable to that of the reaction between superoxide and glutathione. These results suggest both a free-radical scavenging role for the ovothiols and a mechanism by which the ovothiols confer NAD(P)H–O_2 oxidoreductase activity upon the enzyme ovoperoxidase. Investigation of this mechanism implicates the ovothiol thiyl radical and the NAD radical as key intermediates. The ovothiyl radical appears to be unreactive toward oxygen but highly reactive toward NADH. An estimate of the one-electron oxidation potential of the ovothiol anion is presented. The physical basis for the stability of the ovothiol free radical is discussed.

The ovothiols (**1a–c**) are a family of 4-mercaptohistidine derivatives present in the eggs of a variety of marine invertebrates. Ovothiols A and C (**1a** and **1c**), and the parent compound 4-mercaptohistidine, were first isolated (Palumbo et al., 1984; Rossi et al., 1985) from the eggs of echinoderms and molluscs. Turner et al. (1987) subsequently isolated ovothiol B (**1b**) and corrected an error in the earlier structure elucidation work. Studies of the ovothiol content of various tissues (Turner et al., 1987; Rossi et al., 1985) revealed that

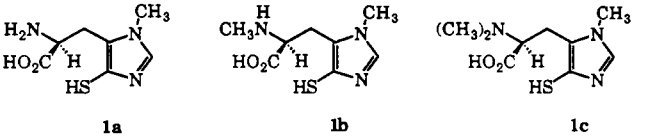

1a **1b** **1c**

† This work was supported by the Searle Scholars Program and the National Institutes of Health (GM 35466). P.B.H. is a Sloan Fellow (1988–1992) and an NIH Research Career Development Award recipient (AG 00417).

0006-2960/90/0429-1953$02.50/0
